Heliyon 10 (2024) e40444

Contents lists available at ScienceDirect

Heliyon

journal homepage: www.cell.com/heliyon

Research article

Pyrazole derivatives as antileishmanial agents: Biological evaluation, molecular docking study, DFT analysis and ADME prediction

Razieh Sabet [a,1], Gholamreza Hatam [b,1], Leila Emami [c,1], Elaheh Ataollahi [c], Fateme Zare [c], Leila Zamani [c], Behnaz Kazemi [d], Masood Mohabati Jahromi [d], Sara Sadeghian [a,*], Soghra Khabnadideh [a,c,**]

[a] Department of Medicinal Chemistry, School of Pharmacy, Shiraz University of Medical Sciences, Shiraz, Iran
[b] Basic Sciences in infectious diseases Research Center, Shiraz University of Medical Sciences, Shiraz, Iran
[c] Pharmaceutical Sciences Research Center, Shiraz University of Medical Sciences, Shiraz, Iran
[d] Student Research Committee, School of Pharmacy, Shiraz University of Medical Sciences, Shiraz, Iran

ARTICLE INFO

Keywords:
Pyrazole
Antileishmanial
Molecular docking
DFT analysis
ADME prediction

ABSTRACT

Leishmaniasis is a parasitic disease that is commonly found in tropical and sub-tropical regions. Currently, there is no protective antileishmanial vaccine, and the available clinical drugs have serious side effects. On the other hand, due to the emergence of multidrug-resistant strains of the causative pathogens, the study and design of novel antileishmanial agents is urgently needed. Accordingly, fourteen previously synthesized pyrazole and pyrano [2,3-c] pyrazole derivatives **(P_1-P_{14})** were evaluated for antileishmanial efficacy against the protozoan parasite, *Leishmania major*. Among the tested compounds, seven derivatives including **P_1**, **P_3**, **P_5**, **P_8**, **P_{12}**, **P_{13}**, and **P_{14}** exhibited promising antileishmanial activity with IC_{50} values in the range of 34.79–43.55 μg/mL, compared to the standard drug (Glucantime) with an IC_{50} value of 97.31 μg/mL. In the case of pyrazole derivatives, **P_1**, **P_5**, and **P_8** exhibited significant antileishmanial activity with IC_{50} values of 35.53, 36.79, and 37.40 μg/mL, respectively. The most potent antileishmanial activity is belong to **P_{12}** and **P_{14}**, with IC_{50} values of 34.79 and 38.51 μg/mL, respectively. Molecular docking outputs presented that **P_{12}** and **P_{14}** formed favorable interactions with key residues in the active site of the 14-alpha demethylase enzyme, which is an important target for antileishmanial agents. Various DFT parameters were also calculated for compounds **P_1** and **P_{12}**, which were the most and least active compounds, respectively. The outputs indicated that compound **P_1** was more thermodynamically stable than **P_{12}**. Additionally, **P_1** had higher hardness and a higher energy gap, resulting in greater stability. In addition, these compounds showed satisfactory theoretical ADME properties. The present results indicate that the investigated pyrazole and pyrano [2,3-c] pyrazole derivatives can be considered as promising agents for the development of antileishmaniasis treatments.

* Corresponding author.
** Corresponding author. Department of Medicinal Chemistry, School of Pharmacy, Shiraz University of Medical Sciences, Shiraz, Iran.
E-mail addresses: s_sadeghian@sums.ac.ir (S. Sadeghian), khabns@sums.ac.ir (S. Khabnadideh).
[1] These authors contributed equally to this work.

https://doi.org/10.1016/j.heliyon.2024.e40444
Received 14 April 2024; Received in revised form 27 October 2024; Accepted 13 November 2024
Available online 19 November 2024

1. Introduction

Leishmaniasis is a highly prevalent and chronic intracellular infectious disease caused by the protozoan parasites of the genus *Leishmania*, which can lead to a wide range of symptoms in humans, from asymptomatic infection to serious problems with visceral, cutaneous, and mucocutaneous symptoms [1-3]. Leishmaniasis is recognized by the World Health Organization (WHO) as the second most important tropical protozoan disease, following malaria [4-7]. The disease is endemic in the tropical and subtropical regions of 98 countries across four continents [8]. The clinical forms of leishmaniasis include Cutaneous (CL), Mucocutaneous (MCL), Visceral (VL) Post-Kala-Azar Dermal (PKDL), and Diffuse Cutaneous (DCL) leishmaniasis. More than 90 % of CL cases is present in Iran, Afghanistan, Nepal, Syria, Saudi Arabia, and Peru [9]. Leishmaniasis, as one of the most significant tropical diseases that puts approximately 350 million people at risk of infection, has been neglected in terms of drug discovery [1,2]. Currently, there is no approved vaccine available for humans, and the treatment of this disease is limited to miltefosine, pentamidine, paromomycin, liposomal amphotericin B, and pentavalent antimonials like sodium stibogluconate [2,4,10]. Furthermore, the drugs used to treat cutaneous and visceral leishmaniasis are associated with severe toxicity and side effects, and the emergence of resistance limits their use [11-13]. Consequently, the pursuit of novel, cost-effective, and safe pharmacological agents with minimal adverse effects for the treatment of leishmaniasis are a significant challenge for researchers on a global scale.

Heterocyclic compounds with a cyclic ring system have different biological potential, special in the inhibition of numerous infections [14]. Nitrogen-containing heterocyclic compounds have predominantly been documented as bioactive agents that exhibit different biological potential, such as antimalarial, antibacterial, antileishmanial, antifungal, anticonvulsant, anti-inflammatory, anthelmintic, analgesic, and anticancer properties [15-19]. Among heterocyclic compounds, azoles are inhibitors of the 14-alpha demethylase enzyme, which is a promising target for the treatment of both leishmaniasis and fungal diseases. Leishmania, similar to fungi, has 24-substituted sterols like ergosterol as a crucial component in its membrane structure. Preventing the production of leishmanial ergosterol can lead to the disruption of membrane stability and the death of Leishmania [20-22].

Pyrazole derivatives are a significant category of bioactive azole compounds [23-31]. Previous studies have shown that pyrazole derivatives can inhibit ergosterol biosynthesis. Ergosterol is an attractive target for the treatment of leishmaniasis. In recent years, some pyrazole derivatives have been reported as antileishmanial agents [32-37]. Accordingly, in this study we investigated the antileishmanial effects of pyrazole and pyrano [2,3-c] pyrazole derivatives.

Recently, different derivatives of 1,2,4-trioxolane-pyrazole and 1,2,4,5-tetraoxane-pyrazole (Structure I) were examined as antileishmanial agents. The biological evaluation of these hybrids showed that some of the compounds had promising activity against *L. tropica* [38]. The *in vitro* antileishmanial activities of hydrazine-coupled pyrazole derivatives were examined. The results revealed that some of the compounds showed superior antipromastigote activity (IC_{50} = 0.018 μg/mL) (Structure II) (Fig. 1) [39].

So, in view of important biological activities of pyrazole moiety as antileishmanial agents, we reported the synthesis and biological evaluation of some pyrazole and pyrano [2,3-c]pyrazole compounds in our previous studies [40,41]. Herein, we aimed to investigate the *in vitro* antileishmanial activity of a series of pyrazole and pyrano [2,3-c]pyrazole derivatives against *Leishmania major promastigotes* (MRHO/IR /75/ER) using the MTT assay. Furthermore, molecular docking study, DFT analysis, and the theoretical investigation of ADME properties were performed to obtain structural information related to the antileishmanial activity of these compounds.

2. Results and discussion

2.1. In vitro antileishmanial activity

The pyrazole and pyrano [2,3-c] pyrazole derivatives **P_1-P_{14}**, which were evaluated in this study, were previously synthesized by our research group according to the synthetic method outlined in Fig. 2 [40,41].

The *in vitro* antileishmanial activities of all pyrazole and pyrano [2,3-c] pyrazole derivatives **P_1-P_{14}** were evaluated against *Leishmania major* promastigotes (MRHO/IR/75/ER) using the MTT assay. The obtained IC_{50} values for all compounds, defined as the concentration that reduces 50 % of cell growth, are depicted in Fig. 3. In this assay, Glucantime, an antileishmanial drug, was used as a positive control.

Based on the obtained biological results, the tested compounds **P_1-P_{14}** showed different levels of antileishmanial activities with IC_{50} ranging from 34.79 to >288 μg/mL. Among all the tested compounds, **P_1, P_3, P_5, P_8, P_{12}, P_{13},** and **P_{14}** exhibited the highest activities

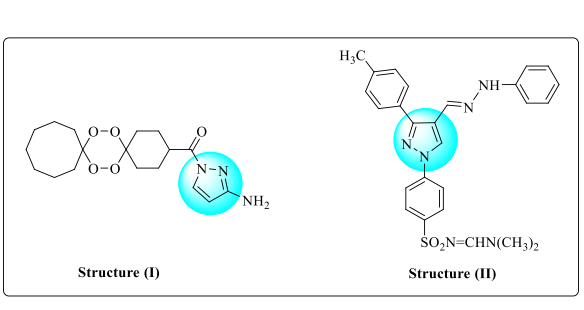

Fig. 1. Structures of some reported antileishmanial agents.

as antileishmanial agents with IC_{50} values of 34.79–43.55 μg/mL, which were 2–3 times more effective than Glucantime, as the control drug. Other compounds including **P_2**, **P_4**, **P_6**, **P_7**, **P_9**, **P_{10}**, and **P_{11}** were inactive with $IC_{50} > 288$ μg/mL.

Compound **P_1**, bearing a pyrazole ring without any substitution on the phenyl ring, showed an IC_{50} value of 35.53 μg/mL. Compound **P_{12}**, containing a pyrano [2,3-c] pyrazole ring with 2,4-di-Cl substituents on the phenyl ring at C-4 positio n, exhibited an IC_{50} value of 34.79 μg/mL. Additionally, compounds **P_3**, **P_5**, **P_8**, **P_{13}**, and **P_{14}** showed similar activity to compounds **P_1** and **P_{12}**.

It was observed that both pyrazole and pyrano [2,3-c] pyrazole scaffolds are effective for antileishmanial activity and the nature and position of the substituents placed on these scaffolds significantly affect their activity. In the case of pyrazole derivatives, it was found that the presence of a chlorine group at the C-4 position of the pyrazole ring (**P_3** vs **P_4**) or on the phenyl ring (**P_8**) is favorable for antileishmanial effects. In addition, the presence of 4-Br group (**P_2** vs **P_1**) on the phenyl ring diminish the activity of pyrazole derivatives. In the case of pyran o [2,3-c] pyrazole derivatives placing a phenyl ring with 2,4-di-Cl or 2,4-di-OH substituents (**P_{12}** and **P_{13}**), as well as placing a furan group (**P_{14}**) at C-4 position of pyrano [2,3-c] pyrazole ring is suitable for the effect of these compounds (Fig. 4).

Taken together, the comparison of our results with other reported antileishmanial agents showed that pyrazole and pyrano [2,3-c] pyrazole derivatives are promising scaffolds for development as antileishmanial agents for future studies (Table 1).

2.2. Molecular docking study

For molecular docking studies, the CYP51 enzyme from L. infantum with PDB ID: 3L4D was used. The active site of this enzyme is evident as a channel composed of amino acids with hydrophobic side chains that provides access to the heme group, where the catalytic activity occurs. It has been found that interaction with the heme group in the CYP51 enzyme, especially coordination with the iron, is important for blocking its activity. The reliability of docking protocol was evaluated with redocking procedure and the RMSD value was obtained 0.93 Å which confirmed the validation of the docking protocol.

The molecular docking results (Figs. 5–9 and Table 2) revealed that compounds **P_1**-**P_{14}** were located in the active site of CYP51, and the binding free energy of all compounds was in the range of −6.0 to −9.5 kcal/mol, which was more favorable than that of the positive control (Glucantime, −5.1 kcal/mol).

Hydrogen bonds are essential factors to assess the structure of proteins and nucleic acid. They also play a crucial role in the specificity of enzyme catalysis, biological information transfer, and enzymatic reaction rate [48]. As seen in Table 2, all compounds had strong hydrogen bond interaction due to their distances (≤3.1 Å) except P_8 and P_1 [49]. Hydrogen bonds also have a great impact on the stabilization of enzyme-ligand complexes. Three hydrogen bonds was seen between Glucantime and the residue in the active site of CYP51 enzyme (Fig. 5).

The molecular docking results indicated that most of the studied compounds formed hydrogen bonds with the enzyme active site [50-52]. The target compounds also made additional interactions such as π-sulfur, π-π stacking, and π-sigma interactions, which led to strong interactions with the receptor. Met357 and Phe48 were the key amino acids that formed π-sulfur and π-π stacking interactions in

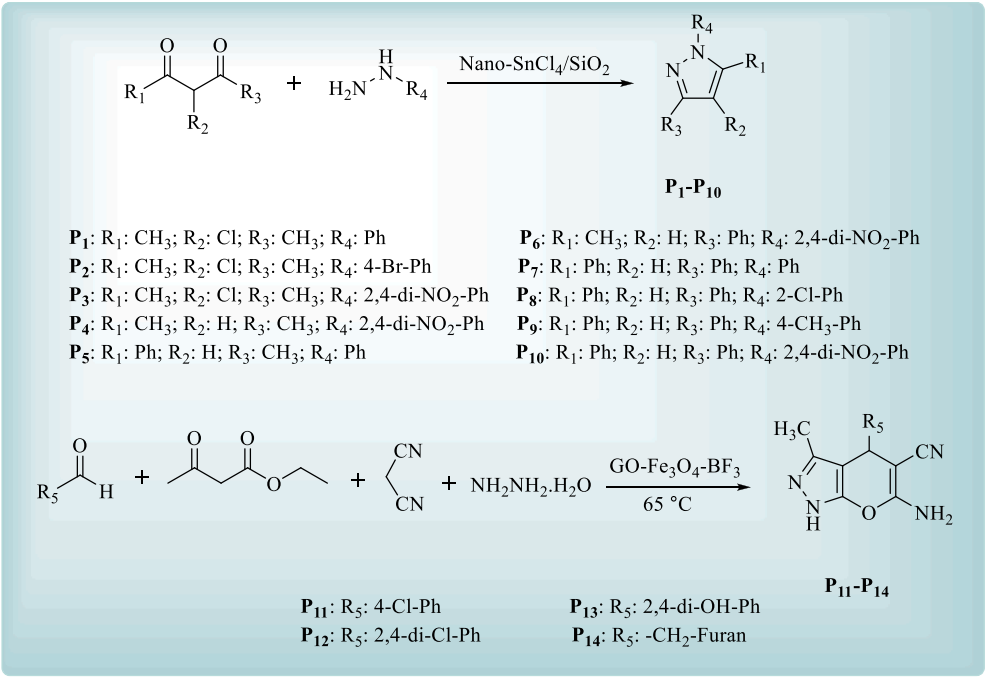

Fig. 2. Synthesis procedure of studied pyrazole and pyrano [2,3-c] pyrazole derivatives.

most of the compounds. **P_1** and **P_{12}**, as the most potent compounds, exhibited one and two hydrogen bonds, respectively, with Cys422, Tyr456, and Thr458 residues, and the binding affinity values of −7.4 and −7.9 kcal/mol, respectively. In addition, **P_1** and **P_{12}** established π-sulfur, π-π stacking, amide π-stacking, and π-alkyl interactions with Phe415, Ala290, Phe48, Phe213, and Met357 residues located within the active site of the CYP51 receptor. Compounds **P_3**, **P_5**, **P_8**, **P_{13}**, and **P_{14}**, as the relatively active compounds, made hydrogen bonds, π-sulfur, π-π stacking, π-sigma, π-anion, π-cation, and π-alkyl interactions with critical residues such as Val356, Met357, His293, Thr294, His420, Phe48, Cys422, Met359, and Glu204 (Figs. 6–7).

Compounds **P_2**, **P_4**, **P_6**, **P_7**, **P_9**, **P_{10}**, and **P_{11}** had weaker interactions with the active site of the enzyme (Figs. 8–9).

2.3. DFT calculations

DFT calculations help to obtain useful information about the structure of the studied molecules and their reactivity. Calculation of the highest unoccupied molecular orbital (LUMO), the lowest occupied molecular orbital (HOMO), and the energy gap between them

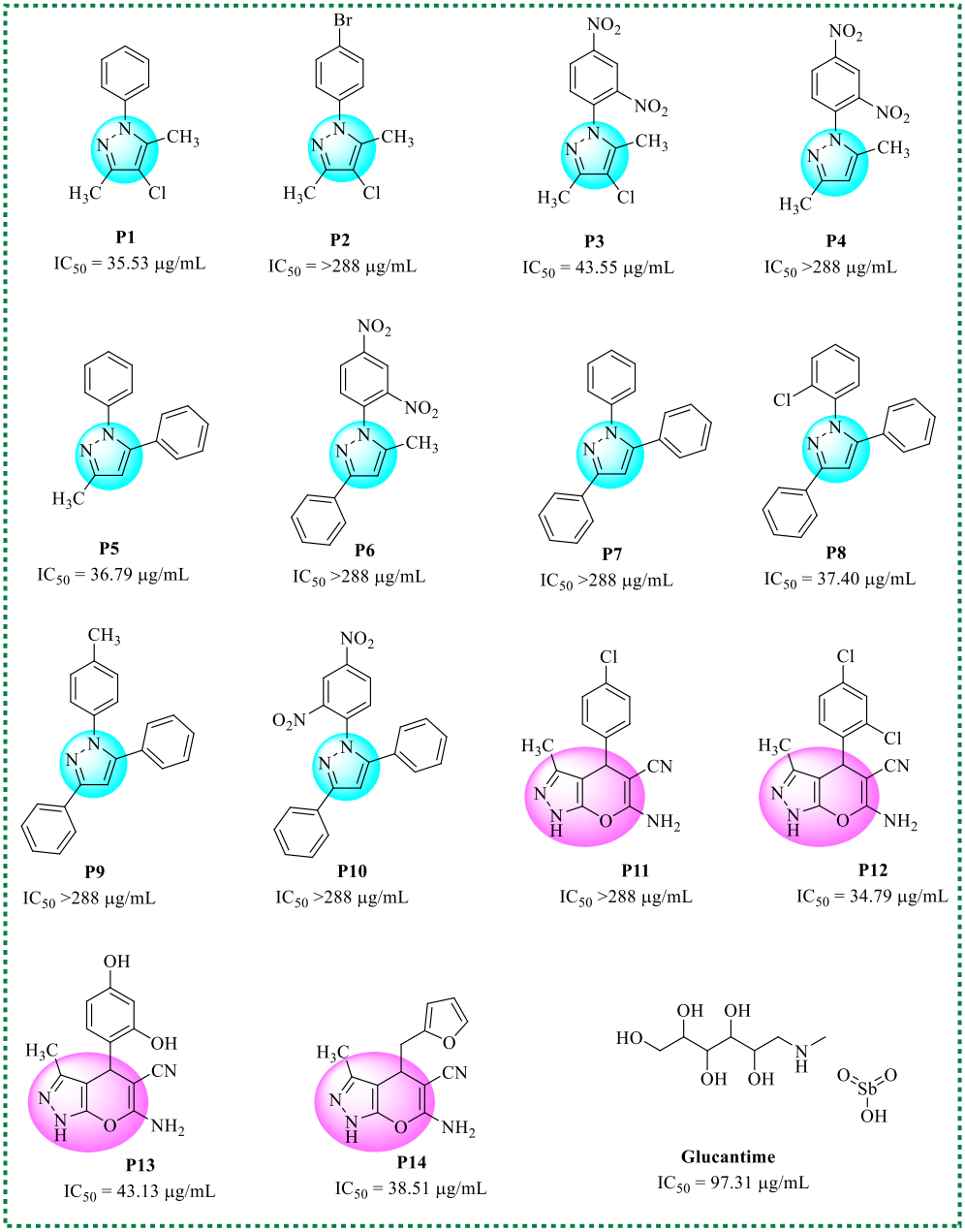

Fig. 3. The chemical structures and antileishmanial activity of the tested compounds **P_1-P_{14}**.

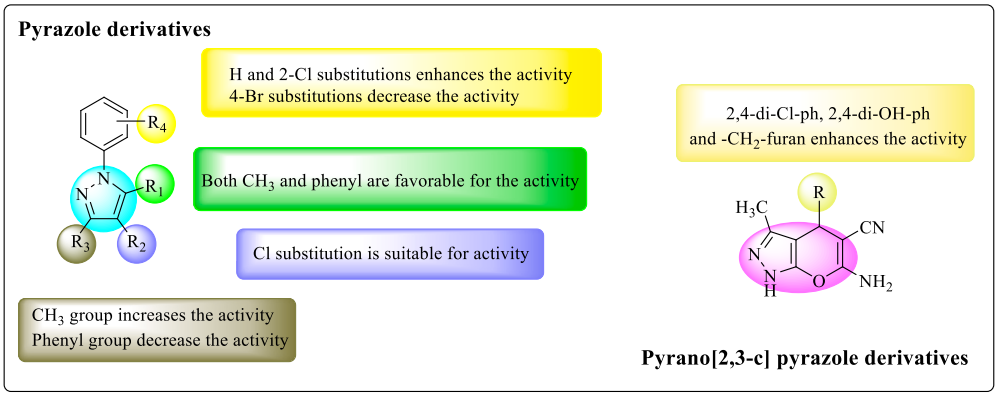

Fig. 4. The schematic SAR of pyrazole and pyrano [2,3-c] pyrazole scaffolds as antileishmanial agents.

Table 1
A comparative study of the inhibition activity of the other reported scaffolds against Leishmanial disease.

Compounds	Antileishmanial activity; IC_{50} (μg/mL or μM)	Compounds	Antileishmanial activity; IC_{50} (μg/mL or μM)
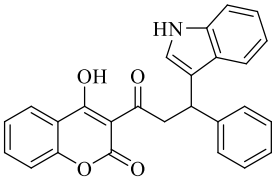	95.5 μg/mL [4]	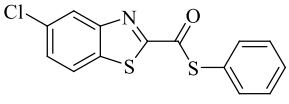	180.0 μM [2]
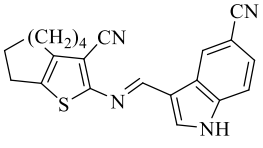	2.1 μg/mL [42]	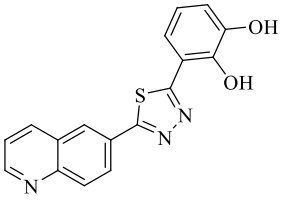	0.04 μM [43]
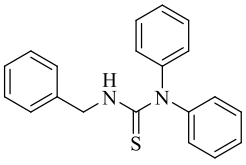	21.4 μM [44]	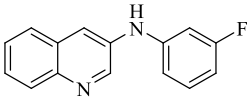	41.9 μM [45]
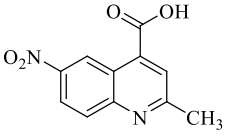	1.49 μg/mL [46]	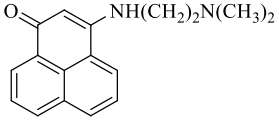	0.6 μM [47]

is one of the parameters that predicate the reactivity and stability of the compounds. DFT analysis was done at the B3LYP/6-31 + G** level of theory for $\mathbf{P_1}$ and $\mathbf{P_{12}}$, as the best molecules according to the biological results using Gaussian 09 software.

The HOMO and LUMO orbitals, their energies, and locations on the studied molecules are shown in Fig. 10. For compound $\mathbf{P_{12}}$ (Fig. 10b), the LUMO orbital covers the entire molecule, and the HOMO orbital is occupied in all parts of the molecule except for a part of the dichlorophenyl ring. In addition, for molecule $\mathbf{P_1}$ (Fig. 10a), the HOMO and LUMO orbitals are distributed throughout the molecule, indicating that all parts of the molecule can be targeted by electrophilic and nucleophilic compounds. The energy gap between HOMO and LUMO was calculated to be 5.44 and 4.75 ev for $\mathbf{P_1}$ and $\mathbf{P_{12}}$, respectively. A higher energy gap indicates more stability, while a lower energy gap indicates more reactivity. Therefore, according to the energy gap values of the two compounds, compound $\mathbf{P_1}$, with a larger energy gap, is more stable.

The nucleophilic and electrophilic sites of compounds were determined by the electrostatic potential map (ESP). Fig. 11 was showed the ESP maps of $\mathbf{P_{12}}$ and $\mathbf{P_1}$ derivatives. Red spheres indicate preferred sites for electrophilic attack, while blue spheres are

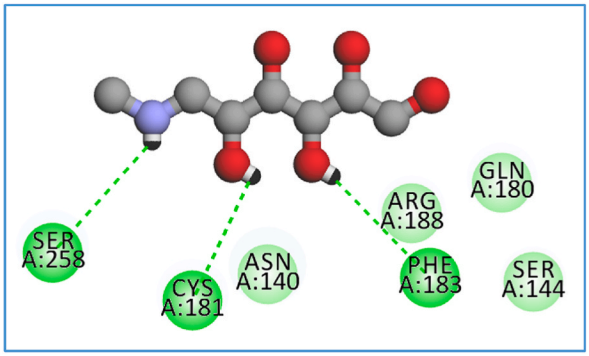

Fig. 5. Interactions of Glucantime in the active site of CYP51 receptor.

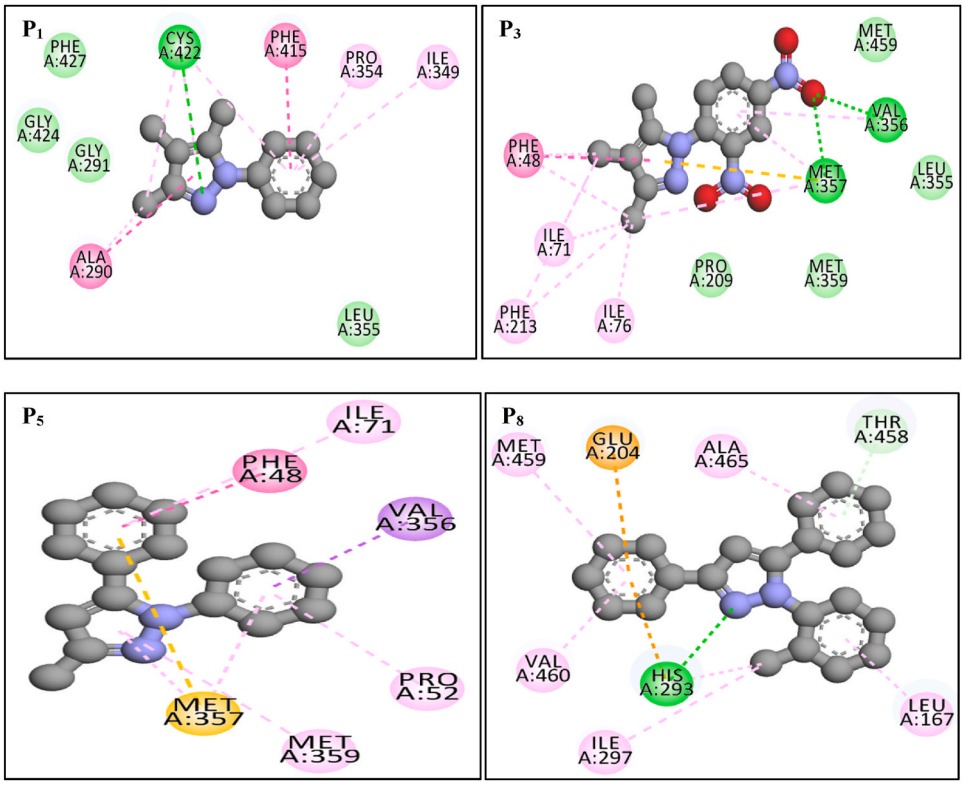

Fig. 6. The two-dimensional interactions of the active compounds $\mathbf{P_1}$, $\mathbf{P_3}$, $\mathbf{P_5}$, and $\mathbf{P_8}$ within the active site of the CYP51 receptor. The interactions are categorized as follows: green represents van der Waals forces, light green denotes carbon-hydrogen bonds, dark green indicates hydrogen bonds, dark pink corresponds to π-π interactions, light pink signifies alkyl and π-alkyl interactions, purple reflects π-sigma interactions, and orange illustrates π-sulfur interactions.

suitable sites for nucleophilic attack.

The thermochemistry parameters for $\mathbf{P_1}$ and $\mathbf{P_{12}}$ are given in Table 3. The obtained values of total energy (E), enthalpy (H°), and Gibbs free energy (G°) presented that $\mathbf{P_1}$ was more thermodynamically stable than $\mathbf{P_{12}}$. Chemical hardness (η) expresses the molecular resistance against the deformation of the electron cloud, which is related to the stability of the compound. The hardness parameter is measured through the energy gap between HOMO and LUMO orbitals. The harder the molecule, the wider the HOMO-LUMO gap, and the more stable the molecule. As can be observed in Table 3, compound $\mathbf{P_1}$ has higher chemical hardness compared to compound $\mathbf{P_{12}}$, therefore, it is more stable and less reactive. The electron affinity parameter (A) is also given in Table 3. The calculated values showed the greater tendency of compound $\mathbf{P_{12}}$ to participate in electrophilic reactions.

The theoretical IR spectrum of compounds $\mathbf{P_1}$ and $\mathbf{P_{12}}$ is shown in Fig. 12. The IR peaks of C=C, C-O, C-N, C-Cl, and C-H (aliphatic and aromatic) are well visible and comparable with experimental results.

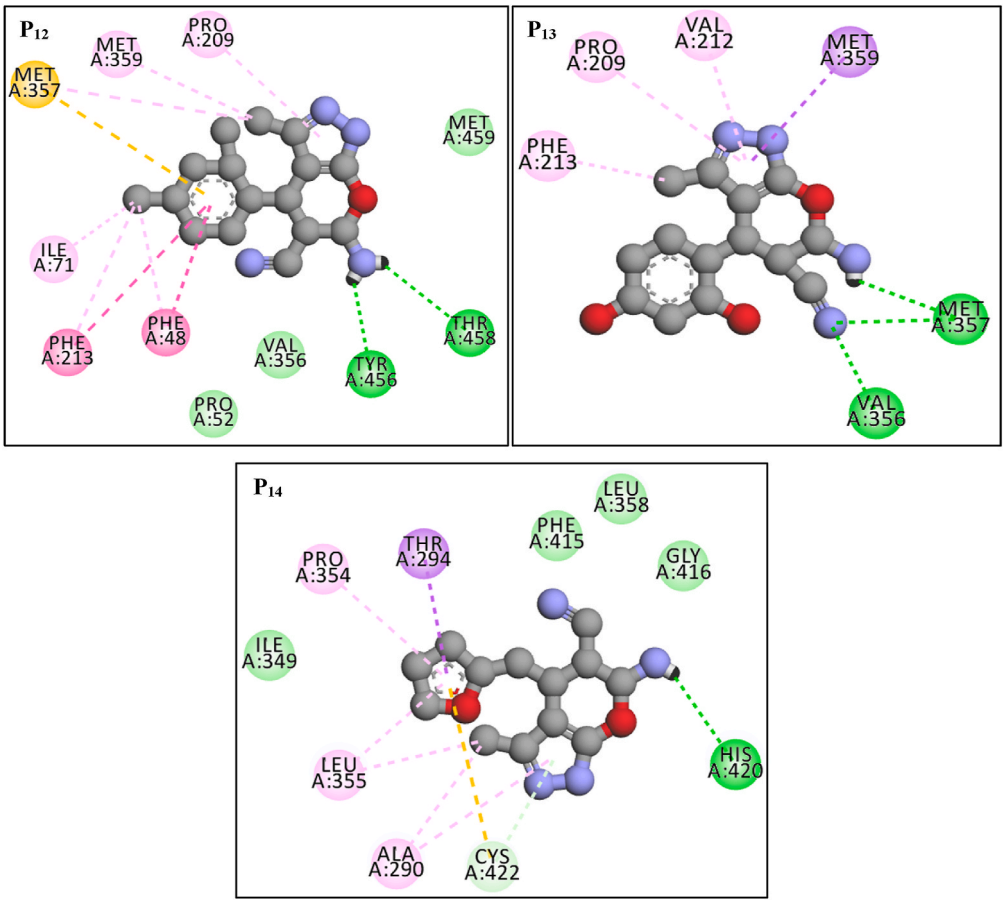

Fig. 7. 2D interactions of the active compounds $\mathbf{P_{12}}$, $\mathbf{P_{13}}$, and $\mathbf{P_{14}}$ within the active site of the CYP51 receptor. The interactions are categorized as follows: green represents van der Waals forces, light green denotes carbon-hydrogen bonds, dark green indicates hydrogen bonds, dark pink corresponds to π-π interactions, light pink signifies alkyl and π-alkyl interactions, purple reflects π-sigma interactions, and orange illustrates π-sulfur interactions.

2.4. ADME profile prediction

The drug-likeness properties of the tested compounds displayed that all the tested derivatives passed Lipinski's rule of five. Compounds $\mathbf{P_1}$, $\mathbf{P_2}$, $\mathbf{P_5}$, $\mathbf{P_7}$, $\mathbf{P_8}$, and $\mathbf{P_9}$ with TPSA (Topological Polar Surface Area) values less than 60 A^2, can be completely absorbed, while the absorption of other compounds with TPSA>60 A^2 is predicted to a lesser degree. Research shows that increasing lipophilicity leads to an increase in the antileishmanial effects of designed compounds [53]. Among all the tested compounds, $\mathbf{P_1}$ and $\mathbf{P_{12}}$ exhibited the expected LogP values (2.87 and 2.28). Furthermore, compounds $\mathbf{P_1}$, $\mathbf{P_3}$, $\mathbf{P_4}$, $\mathbf{P_8}$, $\mathbf{P_{11}}$, and $\mathbf{P_{12}}$ exhibited high permeability, while the other compounds showed low permeability. In addition, all compounds had a negative value of the *in vitro* skin permeability parameter (LogKp), indicating that these derivatives had not skin toxicity. Compound $\mathbf{P_{12}}$ as the most potent compounds showed more negative value of LogKp and the lowest skin toxicity. All compounds except $\mathbf{P_{13}}$ and $\mathbf{P_{14}}$ showed plasma protein binding (PPB) value of more than 90 %. Compounds $\mathbf{P_1}$ and $\mathbf{P_{12}}$ as the most potent compounds indicated acceptable toxicity profile. The pharmacokinetic and drug-likeness profiles of these compounds were reported in supporting information file.

3. Experimental

3.1. Chemistry

The selected synthesized compounds were obtained from our previous study [40,41].

3.2. Parasite culture

The strain of *L. major* (MRHO/IR/75/ER was prepared in Shiraz University of Medical Sciences, Iran. After adaptation in biphasic medium transferred to RPMI 1640 supplemented with penicillin (200 IU/mL), streptomycin (100 μg/mL) and 15 % heat-inactivated

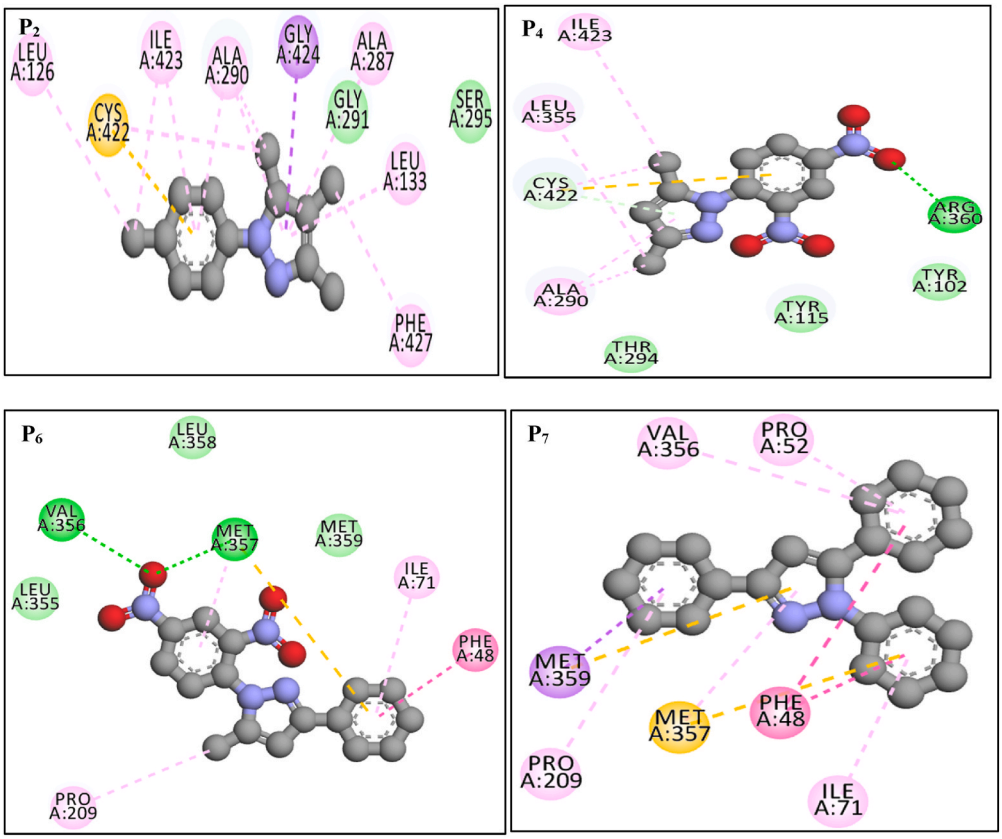

Fig. 8. 2D interactions of compounds $\mathbf{P_2}$, $\mathbf{P_4}$, $\mathbf{P_6}$, and $\mathbf{P_7}$ with the CYP51 receptor. The interactions are categorized as follows: green represents van der Waals forces, light green denotes carbon-hydrogen bonds, dark green indicates hydrogen bonds, dark pink corresponds to π-π interactions, light pink signifies alkyl and π-alkyl interactions, purple reflects π-sigma interactions, and orange illustrates π-sulfur interactions.

fetal calf serum (FCS) for mass cultivation. The L. *major* promastigote cell viability due to the addition of the pyrazole derivatives were determined using the colorimetric MTT assay. The live promastigotes are able to produce the purple formazan crystals with mitochondrial dehydrogenases enzyme.

3.3. Antileishmanial activity

50 μL of a suspension of mass cultivated promastigotes of *L. major* at a density of 10^6 parasites/mL in stationary phase were seaded in culture plates (50,000 parasites/well). For control and blank wells, the same number of promastigotes with solvent and RPMI was applied. Amphotericin B was used in positive control wells and stock solutions of selected synthesized compounds solubilized in DMSO. All four solutions and amphotericin B were sterilized by syringe filters. Different dilutions of compounds were prepared in culture media. Fifty μL of pyrazole compounds diluted in growth medium were added in triplicate. The various concentrations of compounds (5.0, 10.0, 25.0 and 50.0 μg/mL) was prepared and the concentrations of 0.25, 1.0, 2.5 and 10.0 μg/mL was examined for amphotericin B. The applied concentration for DMSO (0.25 %) doesn't harmful to the parasites. 80 μL of the media were aspirated and 80 μL of MTT solution (0.5 mg MTT/well) was treated to each well after 48 h. Afterwards, 200 μL of DMSO was added to each well to solubilize the purple precipitate and the CurveExpert software, version 1.3 was used to determine of IC_{50}s values of all compounds.

3.4. DFT calculations

Density functional theory (DFT) was calculated for compounds $\mathbf{P_1}$ and $\mathbf{P_{12}}$ with the highest biological activity at the B3LYP/6-31 + G** level of theory. Optimization of compounds in the gas phase was conducted using the B3LYP model with a 6-31 + G** basis set in the Gaussian 09 program, assisted by Gauss View 6.0, without imposing any symmetry restrictions. Molecular structures were visualized using Avogadro software. After optimization, the HOMO and LUMO energies were obtained and applied to determine molecular properties such as electron affinity (A), chemical hardness (η), and softness (σ).

$E = Et + Er + Ev + Ee$

$H^\circ = E + kBT$

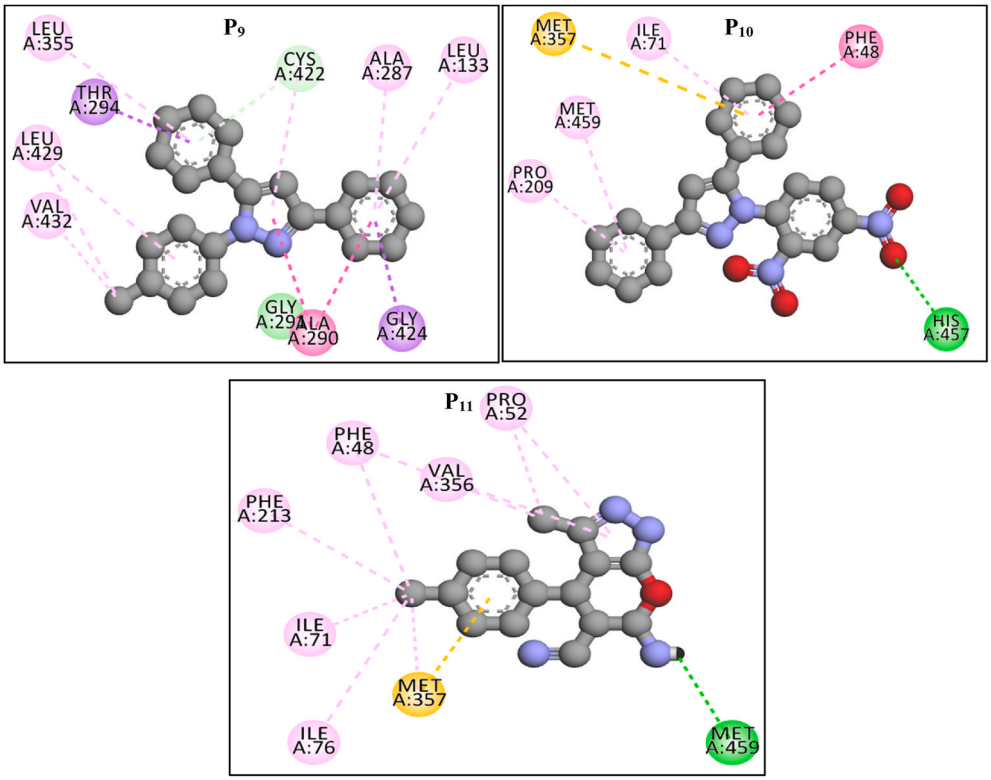

Fig. 9. 2D interactions of compounds **P_9**, **P_{10}**, and **P_{11}** with the CYP51 receptor. The interactions are categorized as follows: green represents van der Waals forces, light green denotes carbon-hydrogen bonds, dark green indicates hydrogen bonds, dark pink corresponds to π-π interactions, light pink signifies alkyl and π-alkyl interactions, purple reflects π-sigma interactions, and orange illustrates π-sulfur interactions.

$G^\circ = H^\circ - TS$

$S = St + Sr + Sv + Se$

$\sigma = 1/\eta$

$\eta = ½ (E_{HOMO} - E_{LUMO})$

$A = - E_{LUMO}$

The vibrational frequencies were also calculated using the B3LYP/6-31 + G** method at the theoretical level. In this regard, electrostatic surface potential (ESP) and some DFT parameters like total energy, enthalpy, entropy, and Gibbs free energy were calculated [54].

3.5. Molecular docking study

The 3D structure of Lanosterol 14α-demethylase (CYP51) was downloaded from the RCSB protein data bank site (PDB ID: 3L4D). From the extracted PDB file, water, ions, internal ligands, and non-polar hydrogens were removed, while polar hydrogens were added. Partial charges were calculated, and the protein was saved in pdbqt format. The size of grid box was set as 40 × 40 × 40 Å dimensions. In the following, the ligands under study were optimized and converted to PDBQT format, and then docked onto the 3L4D using AutoDock Vina (1.1.2) software. The interactions and orientations of pyrazole and pyra no [2,3-c] pyrazole derivatives was visualized by Discovery studio 2016 client.

3.6. ADME study

The physicochemical and drug-likeliness profile of all derivatives were attained from SwissADME online platform (http://www.swiss adme.ch/) in accordance with Lipinski's rules.

Table 2
Binding energy (kcal/mol) and interactions of pyrazole and pyrano [2,3-c] pyrazole derivatives with sterol 14α-demethylase utilizing AutoDock Vina.

Entry	Amino Acid	Ligand involved moiety	Type of interaction and distanced of hydrogen bond interaction (Å)	B.E (kcal/mol)
P_1	Cys 422	Pyrazole ring	Hydrogen Bond (3.45)	−7.4
	Phe 415	Phenyl ring	π- π Stacked	
	Ala 290	Pyrazole ring	Amide π-stacked	
	Ala 290, Ile 349, Pro 354, Cys 422	Pyrazole and phenyl ring, methyl group	Alkyl and π-Alkyl	
	Gly 291, Leu 355, Gly 424, Phe 427	–	Van Der Waals	
P_2	Gly 424	Pyrazole ring	π-Sigma	−7.2
	Cys 422	Phenyl ring	π-Sulfur	
	Leu 126, Leu 133, Ala 287, Ala 290, Cys 422, Ile 423, Phe 427	Methyl, Chlorine, Bromine, Phenyl and pyrazole ring	Alkyl and π-Alkyl	
	Gly 291, Ser 295		Van Der Waals	
P_3	Val 356, Met 357	NO_2 group	Hydrogen Bond Val 356(2.30), Met 357(2.05)	−7.6
	Met 357	Pyrazole ring	π-Sulfur	
	Phe 48	Pyrazole ring	π- π Stacked	
	Phe 48, Ile 71, Ile 76, Phe 213, Val 356, Met 357	Methyl, Chlorine and phenyl ring	Alkyl and π-Alkyl	
	Pro 209, Leu 355, Met 359, Met 459	–	Van Der Waals	
P_4	Arg 360	NO_2 group	Hydrogen Bond	−6.8
	Cys 422	Pyrazole ring	π-Sulfur	
	Cys 422	Pyrazole ring	π-Donor Hydrogen Bond (2.04)	
	Ala 290, Leu 355, Cys 422, Ile 423	Methyl and Pyrazole ring	Alkyl and π-Alkyl	
	Tyr 102, Tyr 115, Thr 294	–	Van Der Waals	
P_5	Val 356	Phenyl ring	π-Sigma	−8.1
	Met 357	Phenyl and pyrazole ring	π-Sulfur	
	Phe 48	Phenyl ring	π- π Stacked	
	Pro 52, Ile 71, Met 357, Met 359	Phenyl and pyrazole ring	π-Alkyl	
P_6	Val 356, Met 357	NO_2 group	Hydrogen Bond Val 356 (1.98), Met 357 (2.90)	−8.8
	Met 357	Phenyl ring	π-Sulfur	
	Phe 48	Phenyl ring	π- π Stacked	
	Ile 71, Pro 209, Met 357	Methyl and Phenyl ring	Alkyl and π-Alkyl	
	Leu 355, Leu 358, Met 359	–	Van Der Waals	
P_7	Met 359	Phenyl ring	π-Sigma	−6.3
	Met 357, Met 359	Phenyl and pyrazole ring	π-Sulfur	
	Phe 48	Phenyl ring	π- π Stacked	
	Phe 48	Phenyl ring	π- π T-shaped	
	Pro 52, Ile 71, Pro 209, Val 356, Met 357	Phenyl and pyrazole ring	π-Alkyl	
P8	His 293	Pyrazole ring	Hydrogen Bond (2.57)	−9.5
	His 293	Phenyl ring	π-Cation	
	Glu 204	Phenyl ring	π-Anion	
	Thr 458	Phenyl ring	π-Donor Hydrogen Bond	
	Leu 167, His 293, Ile 297, Met 459, Val 460, Ala 465	Chlorine and phenyl ring	Alkyl and π-Alkyl	
P_9	Thr 294, Gly 424	Phenyl ring	π-Sigma	−7.2
	Cys 422	Phenyl ring	π-Donor Hydrogen Bond (2.35)	
	Ala 290	Phenyl and pyrazole ring	Amide π-stacked	
	Leu 133, Ala 287, Leu 355, Cys 422, Leu 429, Val 432	Methyl group Phenyl and pyrazole ring	Alkyl and π-Alkyl	
	Gly 291	–	Van Der Waals	
P_{10}	His 457	NO_2 group	Hydrogen Bond (2.39)	−6.7
	Met 357	Phenyl ring	π-Sulfur	
	Phe 48	Phenyl ring	π- π Stacked	
	Ile 71, Pro 209, Met 459	Phenyl ring	π-Alkyl	
P_{11}	Met 459	Amine group	Hydrogen Bond (2.14)	−7.4
	Met 357	Phenyl ring	π-Sulfur	
	Phe 48, Pro 52, Ile 71, Ile 76, Phe 213, Val 356, Met 357	Chlorine and methyl groups Pyrazole ring	Alkyl and π-Alkyl	
P_{12}	Tyr 456, Thr 458	Amine group	Hydrogen Bond Tyr 456 (2.04), Thr 458 (2.49)	−7.9
	Met 357	Phenyl ring	π-Sulfur	
	Phe 48, Phe 213	Phenyl ring	π- π Stacked	
	Phe 48, Ile 71, Pro 209, Phe 213, Met 357, Met 359	Methyl, pyrazole, and Cl moiety	Alkyl and π-Alkyl	
	Pro 52, Val 356, Met 459	–	Van Der Waals	
P_{13}	Val 356, Met 357	NO_2 and CN groups	Hydrogen Bond Val 356 (2.09), Met 357 (2.06)	−7.4

(*continued on next page*)

Table 2 (*continued*)

Entry	Amino Acid	Ligand involved moiety	Type of interaction and distanced of hydrogen bond interaction (Å)	B.E (kcal/mol)
	Met 359	Pyrazole ring	π-Sigma	
	Pro 209, Val 212, Phe 213	Methyl and pyrazole ring	π-Alkyl	
P_{14}	His 420	Amine group	Hydrogen Bond	−7.2
	Thr 294	Furan ring	π-Sigma	
	Cys 422	Furan ring	π-Sulfur	
	Cys 422	Furan ring	π-Donor Hydrogen Bond (2.42)	
	Ala 290, Pro 354, Leu 355	Methyl group, pyrazole and furan rings	Alkyl and π-Alkyl	
	Ile 349, Leu 358, Phe 415, Gly 416	–	Van Der Waals	
Glucantime	Amine and hydroxy group	Cys 181, Phe 183, Ser 258	Hydrogen bond	−5.1
	–	Asn 140, Ser 144, Gln 180, Arg 188	Van Der Waals	

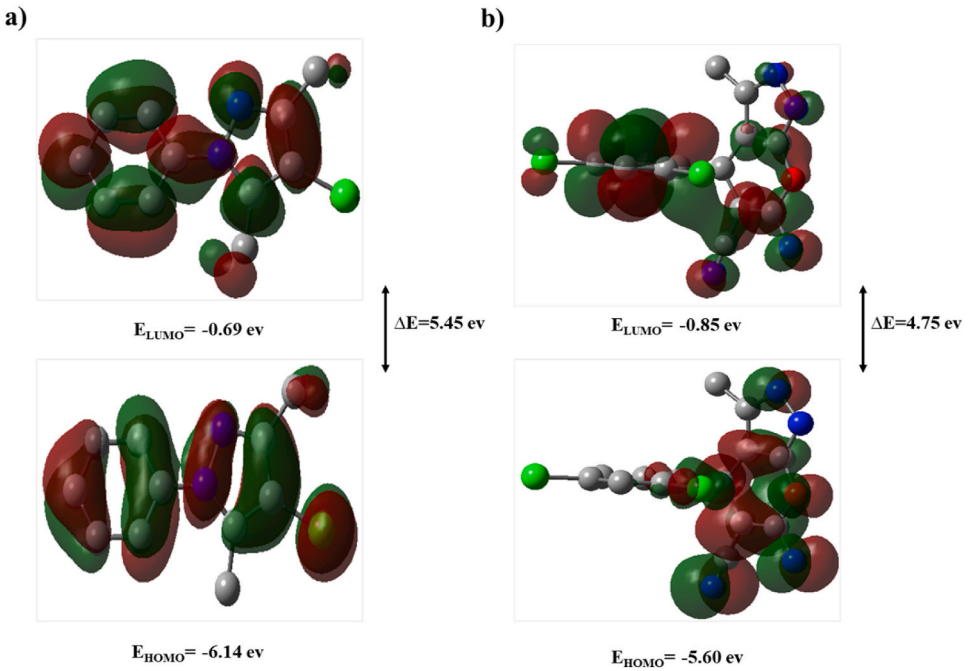

Fig. 10. LUMO, HOMO, and their energies diagram for $\mathbf{P_1}$ (left) and $\mathbf{P_{12}}$ (right) at the B3LYP/6-31 + G** level of theory.

3.7. Implications of findings and suggestions for future researches

Zoonotic cutaneous leishmaniasis is a neglected tropical infectious disease caused by an important species of the genus Leishmania, known as *L. major* that has affected many parts of tropical and subtropical regions [14]. Considering the lack of an effective vaccine so far and the limitation of drug treatments due to the occurrence of resistance or the presence of harmful side effects, the need for comprehensive investigations to obtain new drugs is quite noticeable. In this study, different derivatives of pyrazoles were first checked in terms of cytotoxicity in the cell culture environment and the effect of their non-toxic doses on the parasite was investigated in the *in vitro* environment.

It is apparent that the presence chloro group at position 4 of pyrazole moiety is more favorable and also, introducing nitro groups at phenyl ring resulted in enhancement the activity. On the other hand, in compounds that don't featuring chloro substitutions, the incorporation of at least two phenyl motif is necessary. Fortunately, one of the derivatives that showed more thermochemical resistance showed good lethality on promastigotes. It is necessary to enter this compound into an animal study on Balb/c inbred mice in the next step and if we get the right results, we will design a clinical trial to examine its effect on patients.

4. Conclusion

In summary, a new set of pyrazole and pyrano [2,3-c] pyrazole derivatives were evaluated for their antileishmanial activity. Among of all tested compounds, $\mathbf{P_1}$, $\mathbf{P_3}$, $\mathbf{P_5}$, $\mathbf{P_8}$, $\mathbf{P_{12}}$, $\mathbf{P_{13}}$, and $\mathbf{P_{14}}$ were found to possess a promising antileishmanial activity with IC_{50} values in a range of 34.79–43.55 μg/mL, which were 2–3 times more effective compared with Glucantime, the control drug (IC_{50} = 97.31 μg/

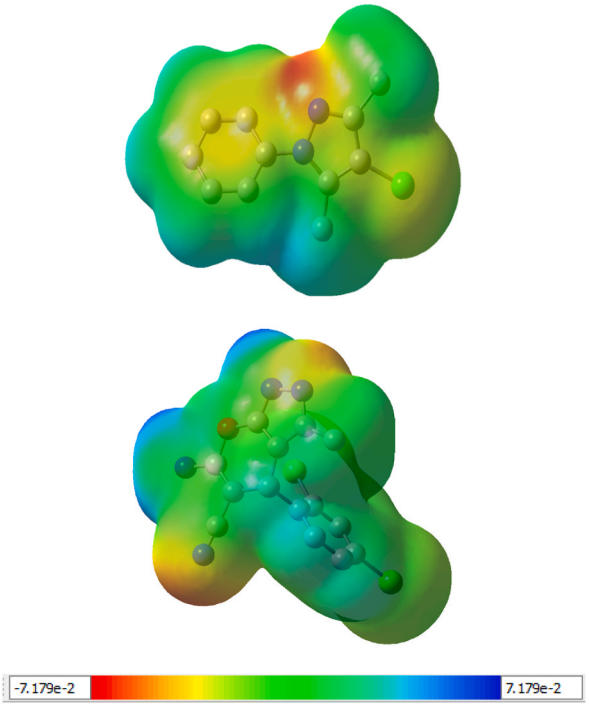

Fig. 11. Electrostatic potential maps for $\mathbf{P_1}$ (left) and $\mathbf{P_{12}}$ (right) at B3LYP/6-31 + G (d,p) level of theory.

Table 3
The some DFT indices of $\mathbf{P_1}$ and $\mathbf{P_{12}}$ at B3LYP/6-31 + G** level of theory.

Entry	E_{tot}[a]	H°[a]	G°[a]	S[b]	η[c]	σ[d]	A[c]
$\mathbf{P_1}$	−1744.84	−1744.84	−1744.91	140.76	2.72	0.36	0.69
$\mathbf{P_{12}}$	−990.12	−990.12	−990.17	112.24	2.52	0.39	0.85

[a] in Hartree/particle.
[b] in cal/mol.K.
[c] in ev.
[d] in ev^{-1}.

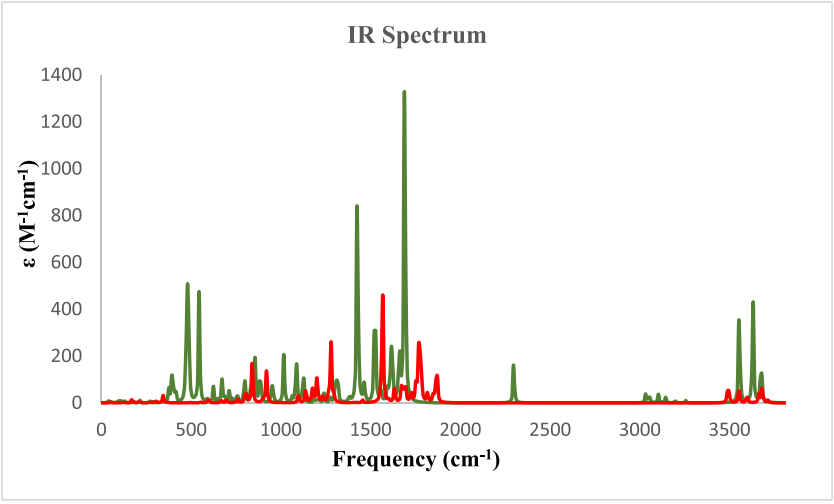

Fig. 12. Calculated IR spectra for $\mathbf{P_1}$ (red) and $\mathbf{P_{12}}$ (green) at B3LYP/6-31 + G** level of theory.

mL). The SAR studies highlighted the significant role of chloro substitution at the C-4 position of pyrazole moiety and the phenyl moiety toward antileishmanial activity. Molecular docking studies also, showed possible binding interaction of the tested derivatives in the active site of CYP51 enzyme, an important target for antileishmanial agents. DFT analysis was performed on the most active compounds, $\mathbf{P_1}$ and $\mathbf{P_{12}}$. The DFT parameters such as energy gap HOMO and LUMO, hardness and softness parameters displayed that $\mathbf{P_{12}}$ had greater stability and lower reactivity than $\mathbf{P_1}$. The theoretical and experimental IR spectra for both compounds showed good agreement. Furthermore, *in silico* ADME properties demonstrated promising physicochemical and pharmacokinetic results for the active compounds. In overall, pyrazole and pyrano [2,3-c] pyrazole compounds are valuable lead scaffolds for further study in order to achieve new antileishmanial agents.

CRediT authorship contribution statement

Razieh Sabet: Project administration. **Gholamreza Hatam:** Project administration. **Leila Emami:** Writing – original draft. **Elaheh Ataollahi:** Writing – original draft, Software. **Fateme Zare:** Writing – original draft. **Leila Zamani:** Methodology. **Behnaz Kazemi:** Investigation. **Masood Mohabati Jahromi:** Investigation. **Sara Sadeghian:** Writing – review & editing. **Soghra Khabnadideh:** Supervision.

Ethics approval and consent to participate

All applicable international, national, and/or institutional guidelines for the care and use of live vertebrates were followed. All procedures performed in studies involving live vertebrates were in accordance with ethical standards of the institution or practice at which the studies were conducted. Procedures involving live vertebrates and their care were done under the ethical guidelines approved by Shiraz University of Medical Sciences, Shiraz, Iran.

Data availability statement

The used and analyzed data sets during the current study are available from the corresponding author upon request. We have showed all data in the form of Tables and Figures.

Declaration of competing interest

The authors declare the following financial interests/personal relationships which may be considered as potential competing interests: Soghra Khabnadideh reports financial support was provided by Shiraz University of Medical Sciences. Soghra Khabnadideh reports a relationship with Shiraz University of Medical Sciences that includes: board membership, employment, and funding grants. If there are other authors, they declare that they have no known competing financial interests or personal relationships that could have appeared to influence the work reported in this paper.

Acknowledgments

This investigation was financially supported by Shiraz University of Medical Sciences, Shiraz, Iran. (Grant No.: 11251).

Appendix A. Supplementary data

Supplementary data to this article can be found online at https://doi.org/10.1016/j.heliyon.2024.e40444.

References

[1] P.F. Espuri, et al., Synthesis and evaluation of the antileishmanial activity of silver compounds containing imidazolidine-2-thione, JBIC Journal of Biological Inorganic Chemistry 24 (2019) 419–432.
[2] A.A. Dar, et al., One-pot synthesis and evaluation of antileishmanial activities of functionalized S-alkyl/aryl benzothiazole-2-carbothioate scaffold, J. Org. Chem. 81 (8) (2016) 3149–3160.
[3] M. Motazedian, et al., A urine-based polymerase chain reaction method for the diagnosis of visceral leishmaniasis in immunocompetent patients, Diagn. Microbiol. Infect. Dis. 60 (2) (2008) 151–154.
[4] J.N. Sangshetti, et al., Antileishmanial activity of novel indolyl–coumarin hybrids: design, synthesis, biological evaluation, molecular docking study and in silico ADME prediction, Bioorg. Med. Chem. Lett 26 (3) (2016) 829–835.
[5] S. Tabrez, et al., Targeting sterol alpha-14 demethylase of Leishmania donovani to fight against leishmaniasis, J. Cell. Biochem. 122 (9) (2021) 1037–1047.
[6] N. Mekarnia, et al., Effect of Phlebotomus papatasi on the fitness, infectivity and antimony-resistance phenotype of antimony-resistant Leishmania major Mon-25, Int. J. Parasitol.: Drugs Drug Resist. 25 (2024) 100554.
[7] E. Schadich, et al., Activity of 1-aryl-4-(naphthalimidoalkyl) piperazine derivatives against Leishmania major and Leishmania mexicana, Parasitol. Int. 91 (2022) 102647.
[8] I. Mohammadpour, et al., Leishmania cytochrome b gene sequence polymorphisms in southern Iran: relationships with different cutaneous clinical manifestations, BMC Infect. Dis. 19 (2019) 1–13.

[9] S. Mirzavand, et al., In vitro and in vivo assessment of anti-leishmanial efficacy of leaf, fruit, and fractions of Juniperus excelsa against axenic amastigotes of Leishmania major and topical formulation in BALB/c mice, Iran. Red Crescent Med. J. 21 (6) (2019).
[10] Foroughi-Parvar, F. and G. Hatam, Vaccines for canine leishmaniasis. Advances in preventive medicine, 2014. 2014.
[11] M. Esteves, et al., Synthesis and biological evaluation of trifluralin analogues as antileishmanial agents, Bioorg. Med. Chem. 18 (1) (2010) 274–281.
[12] M.A. Abdelwahid, et al., Synthesis, characterization, and antileishmanial activity of certain quinoline-4-carboxylic acids, J. Chem. 2019 (2019) 1–9.
[13] O.S. Trefzger, et al., Design, synthesis, antileishmanial, and antifungal biological evaluation of novel 3, 5-disubstituted isoxazole compounds based on 5-nitrofuran scaffolds, Arch. Pharmazie 353 (2) (2020) 1900241.
[14] S. De, et al., Seeking heterocyclic scaffolds as antivirals against dengue virus, Eur. J. Med. Chem. 240 (2022) 114576.
[15] M. Yousuf, et al., Antileishmanial ferrocenylquinoline derivatives: synthesis and biological evaluation against Leishmania donovani, Eur. J. Med. Chem. 124 (2016) 468–479.
[16] A. Tejeria, et al., Substituted 1, 5-naphthyridine derivatives as novel antileishmanial agents. Synthesis and biological evaluation, Eur. J. Med. Chem. 152 (2018) 137–147.
[17] S. Sadeghian, et al., Imidazole derivatives as novel and potent antifungal agents: synthesis, biological evaluation, molecular docking study, molecular dynamic simulation and ADME prediction, J. Mol. Struct. 1302 (2024) 137447.
[18] B. Hassani, et al., Synthesis of 3-hydroxypyridin-4-one derivatives bearing benzyl hydrazide substitutions towards anti-tyrosinase and free radical scavenging activities, RSC advances 13 (46) (2023) 32433–32443.
[19] R. Fazel, et al., Design, synthesis, in silico ADME, DFT, molecular dynamics simulation, anti-tyrosinase, and antioxidant activity of some of the 3-hydroxy-pyridin-4-one hybrids in combination with acylhydrazone derivatives, J. Biomol. Struct. Dyn. (2023) 1–11.
[20] V.K. Marrapu, et al., Synthesis and evaluation of new furanyl and thiophenyl azoles as antileishmanial agents, Eur. J. Med. Chem. 46 (5) (2011) 1694–1700.
[21] R.S. Evangelista, et al., Synthesis and evaluation of the antileishmanial activity of novel eugenol analogs containing 1, 2, 3-triazole fragments against intracellular Leishmania braziliensis, J. Braz. Chem. Soc. 34 (2023) 1810–1824.
[22] S. Sadeghian, et al., Evaluation of antibacterial and anticandidal activities of some imidazole, benzimidazole and benztriazole derivatives, Trends in Pharmaceutical Sciences 8 (2) (2022) 75–84.
[23] T.Z. Abolibda, et al., Synthesis and in silico antiviral activity of novel bioactive thiobarbituric acid based hydrazones and pyrazoles against SARS-CoV-2 main protease (mpro), Polycycl. Aromat. Comp. 43 (8) (2023) 7635–7650.
[24] S. Abu-Melha, et al., Clean grinding technique: a facile synthesis and in silico antiviral activity of hydrazones, pyrazoles, and pyrazines bearing thiazole moiety against SARS-CoV-2 main protease (Mpro), Molecules 25 (19) (2020) 4565.
[25] S. Kakkar, B. Narasimhan, A comprehensive review on biological activities of oxazole derivatives, BMC chemistry 13 (1) (2019) 16.
[26] A.O. Abdelhamid, S.M. Gomha, W.A. El-Enany, Efficient synthesis and antimicrobial evaluation of new azolopyrimidines-bearing pyrazole moiety, J. Heterocycl. Chem. 56 (9) (2019) 2487–2493.
[27] S.M. Gomha, H.M. Abdel-aziz, A.A. El-Reedy, Facile synthesis of pyrazolo [3, 4-c] pyrazoles bearing coumarine ring as anticancer agents, J. Heterocycl. Chem. 55 (8) (2018) 1960–1965.
[28] I.M. Abbas, et al., Synthesis and antimicrobial activity of novel azolopyrimidines and pyrido-triazolo-pyrimidinones incorporating pyrazole moiety, J. Heterocycl. Chem. 54 (6) (2017) 3447–3457.
[29] S.M. Gomha, K.M. Dawood, Synthetic utility of pyridinium bromide: synthesis and antimicrobial activity of novel 2, 4, 6-trisubstituted pyridines having pyrazole moiety, J. Heterocycl. Chem. 54 (3) (2017) 1943–1948.
[30] S.M. Gomha, et al., Synthesis, cytotoxicity evaluation, molecular docking and utility of novel chalcones as precursors for heterocycles incorporating pyrazole moiety, Med. Chem. 14 (4) (2018) 344–355.
[31] M.A. Abdallah, et al., An efficient synthesis of novel pyrazole-based heterocycles as potential antitumor agents, Appl. Sci. 7 (8) (2017) 785.
[32] S.S. Salim, et al., Thiamine hydrochloride as an acid catalyst for the facile green synthesis of pyrazolopyranopyrimidines under aqueous conditions, Res. Chem. Intermed. 48 (12) (2022) 5077–5087.
[33] O. Ebenezer, M. Shapi, J.A. Tuszynski, A review of the recent development in the synthesis and biological evaluations of pyrazole derivatives, Biomedicines 10 (5) (2022) 1124.
[34] M. Ramadan, et al., Substituted pyrazoles and their heteroannulated analogs—recent syntheses and biological activities, Molecules 26 (16) (2021) 4995.
[35] J. Safaei-Ghomi, M. Asgari-Kheirabadi, H. Shahbazi-Alavi, Environmentally benign synthesis of methyl 6-amino-5-cyano-4-aryl-2, 4-dihydropyrano [2, 3-c] pyrazole-3-carboxylates using CeO2 nanoparticles as a reusable and robust catalyst, Z. Naturforsch. B Chem. Sci. 71 (11) (2016) 1135–1140.
[36] Y. Walunj, et al., Synthesis, antimicrobial and ergosterol biosynthesis inhibition activity of clubbed 1, 1′-biphenyl-pyrazole derivatives, New J. Chem. 47 (8) (2023) 3810–3824.
[37] I. Khan, et al., Synthesis of new bis-pyrazole linked hydrazides and their in vitro evaluation as antimicrobial and anti-biofilm agents: a mechanistic role on ergosterol biosynthesis inhibition in Candida albicans, Chem. Biol. Drug Des. 94 (1) (2019) 1339–1351.
[38] P.S. Amado, et al., Synthesis, structure and antileishmanial evaluation of endoperoxide–pyrazole hybrids, Molecules 27 (17) (2022) 5401.
[39] H.G. Berhe, et al., Synthesis, antileishmanial, antimalarial evaluation and molecular docking study of some hydrazine-coupled pyrazole derivatives, BMC chemistry 18 (1) (2024) 9.
[40] S. Khabnadideh, et al., Nano-SnCl4/SiO2 as a catalyst for one-pot synthesis of substituted 1H-pyrazoles as antifungal and cytotoxic agents, Lett. Org. Chem. 17 (6) (2020) 459–465.
[41] L. Amiri-zirtol, et al., A novel and efficient boron-containing magnetic catalyst based on graphene oxide (GO-Fe3O4-BFn) for synthesis of pyrazole and pyranopyrazole derivatives, J. Mol. Struct. (2024) 137868.
[42] M.B. Félix, et al., Antileishmanial activity of new thiophene–indole hybrids: design, synthesis, biological and cytotoxic evaluation, and chemometric studies, Bioorg. Med. Chem. 24 (18) (2016) 3972–3977.
[43] N. Barak Almandil, et al., Synthesis of novel quinoline-based thiadazole, evaluation of their antileishmanial potential and molecular docking studies, Biorg. Chem 85 (2019) 109–116.
[44] G.M. Viana, et al., Antileishmanial thioureas: synthesis, biological activity and in silico evaluations of new promising derivatives, Chem. Pharm. Bull. 65 (10) (2017) 911–919.
[45] S.N. Chanquia, et al., Synthesis and biological evaluation of new quinoline derivatives as antileishmanial and antitrypanosomal agents, Bioorg. Chem. 83 (2019) 526–534.
[46] M.A. Abdelwahid, et al., Synthesis, characterization, and antileishmanial activity of certain quinoline-4-carboxylic acids, J. Chem. 2019 (1) (2019) 2859637.
[47] M.B. Freijo, et al., Design, synthesis and evaluation of amino-substituted 1H-phenalen-1-ones as anti-leishmanial agents, Eur. J. Med. Chem. 143 (2018) 1312–1324.
[48] Hubbard R.E., Haider M.K., Hydrogen bonds in proteins: role and strength, 15 February 2010 https://doi.org/10.1002/9780470015902.a0003011.pub2 (2010).
[49] A. Imberty, et al., Molecular modelling of protein-carbohydrate interactions. Docking of monosaccharides in the binding site of concanavalin A, Glycobiology 1 (6) (1991) 631–642.
[50] T.A. Khan, et al., Evaluation of the antiparasitic and antifungal activities of synthetic piperlongumine-type cinnamide derivatives: booster effect by halogen substituents, ChemMedChem 18 (12) (2023) e202300132.
[51] F. Sharifi, et al., Anti-leishmanial, immunomodulatory and additive potential effect of Piperine on Leishmania major: the in silico and in vitro study of Piperine and its combination, Exp. Parasitol. 254 (2023) 108607.

[52] I.S. Al Nasr, et al., Versatile anti-infective properties of pyrido-and dihydropyrido [2, 3-d] pyrimidine-based compounds, Bioorg. Med. Chem. 90 (2023) 117376.
[53] C.M. Maciel-Rezende, et al., Synthesis and biological evaluation against Leishmania amazonensis of a series of alkyl-substituted benzophenones, Bioorg. Med. Chem. 21 (11) (2013) 3114–3119.
[54] S. De, M.S. Alsaeedi, D. Das, Mechanistic insight into the synergistic role of the dual-surfactant system as a green solvent for deoximation reaction: an experimental and computational analysis, J. Mol. Liq. 400 (2024) 124559.